Hierarchical Stochastic Frequency Constrained Micro-Market Model for Isolated Microgrids

Hierarchical Stochastic Frequency Constrained Micro-Market Model for Isolated Microgrids

Tohid Abedi, Gholamreza Yousefi, *Member, IEEE,* and Miadreza Shafie-khah, *Senior Member, IEEE*

***Abstract*—With the developments of isolated microgrids (IMGs) and prosumers in remote areas, energy trading has become more significant in IMGs. On the other hand, the lack of an upstream network and the system's low inertia could endanger the secure operation of these networks. This paper presents a Micro-Market (μM) model for IMGs with the precise modeling of hierarchical control structure. To deal with the IMG's low inertia and high intermittency of renewable energy sources (RES), the proposed μM manages the active-reactive power and schedules sufficiently primary and secondary active reserves to preserve frequency in a predefined range. In addition, a bidirectional linearized AC power flow is established to schedule the reactive reserve and the proposed model is formulated as a two-stage stochastic mixed-integer linear problem (MILP) to maximize social welfare (SW) during the next 24 hours. To verify the ability of the proposed model, the μM is tested in an IMG based on a CIGRE medium-voltage benchmark system and different operational cases are simulated. The results showed that considering hierarchical control levels and technical issues of the IMG in the proposed model is a cost-effective manner to maximize the social welfare while the secure operation of the IMG is ensured.**

***Index Terms*—Micro-Market, hierarchical control level, isolated microgrid, reserve and energy scheduling, frequency security.**

NOMENCLATURE

Acronyms

MG	Microgrid
IMG	Isolated Microgrid
RES	Renewable Energy Source
DER	Distributed Energy Resource
DG	Distributed Generation
SW	Social Welfare
EMS	Energy Management System
μM	Micro-Market
MSO	Microgrid System Operator
LMP	Locational Marginal Pricing
TTP	Trusted Third Party

Indices and sets

b,b'	Index for buses, $b \in B$
f	Index for linear partitions in linearization, $f \in F$
g	Index for generators, $g \in G$
w,s	Index for wind and solar units, $w \in W, s \in S$
e,l	Index for batteries and loads, $e \in E, l \in L$
ω	Index for scenarios, $\omega \in \Omega$
cl	Index for hierarchical control levels including *primary* and *secondary*, $cl \in CL$
t	Index for time (hour), $t \in T$
d	Index for demand response, $d \in D$
N_b^x	Index for unit x located at bus b, $x \in \{L,G,W,S,D\}$
N_x	Total number of unit x, $x \in \{L,G,W,S,D,T\}$

Parameters

$C_{x,t}^{P}$	Bid price of element ***x*** at hour ***t*** for active power, $x \in \{L,G,W,S,D\}$
$C_{g,t,cl}^{R,P} / C_{g,t,cl}^{R,Q}$	Active/reactive reserve provision cost of unit ***g*** at hour ***t*** and control level ***cl***
C_g^{St}, C_g^{Sd}	Startup and shutdown cost of unit ***g***
P_x^{Min} / P_x^{Min}	Maximum and minimum active power of element ***x***, $x \in \{L,G,W,S,D\}$
Q_x^{Min} / Q_x^{Min}	Maximum and minimum reactive power of element ***x***, $x \in \{L,G,W,S,D\}$
$P_e^{Max,dch}, P_e^{Max,ch}$	Maximum discharge/charge power of battery
SOC_e^{Max}, SOC_e^{Min}	Minimum and maximum rate of SOC (kWh)
$\eta_e^{ch}, \eta_e^{dch}$	Charging/discharging efficiency of battery ***e***
R_g^{Up}, R_g^{Dn}	Ramp-up/ramp-down rate of unit ***g***
T_g^{Up}, T_g^{Dn}	Minimum up/down tine of unit ***g***
$\alpha_{w,t}, \alpha_{s,t}$	Maximum available power coefficient for wind and solar units at hour ***t***
$R_{g,t}^{Up_{Max}}, R_{g,t}^{Dn_{Max}}$	Maximum up/downward active reserve power of unit ***g*** at hour ***t***
$Q_{g,t}^{Up_{Max}}, Q_{g,t}^{Dn_{Max}}$	Maximum up/downward reactive reserve power reserve of unit **g** at hour ***t***
$R_{b,b'}, X_{b,b'}$	Resistance/reactance of branch b,b'
$V_{rated}, V_{\min}, V_{\max}$	Nominal/minimum/maximum voltage
$I_{\max,b,b'}$	Maximum allowable current of branch b,b'
r_g	Droop gain of unit ***g***
f_{ref}	Reference frequency in MG
$\Delta f_{cl}^{\max}$	Maximum allowable frequency excursion at control level ***cl***
T	Operating horizon (24 hours)
π_ω	Probability of scenario ω
U_0 / S_0	Time periods unit has been on/off at the beginning of the operating horizon (h)
$U_{g,0}$	Initial status of unit ***g***
ζ_g	Number of initial periods that unit ***g*** must be online/off-line

Variables

$P_{x,t}$	Active power of ***x*** at hour ***t*** $x \in \{L,G,W,S,D\}$
$Q_{x,t}$	Reactive power to ***x*** at hour ***t*** $x \in \{L,G,W,S,D\}$
$P_{x,t,\omega,cl}$	Active power of ***x*** in scenario ω at hour ***t*** and control level ***cl***, $x \in \{L,G,W,S,D\}$
$Q_{x,t,\omega,cl}$	Reactive power of ***x*** in scenario ω at hour ***t*** and control level ***cl*** $x \in \{L,G,W,S,D\}$

(*Corresponding authors: G. Yousefi; M. Shafie-khah*).
T. Abedi and G. Yousefi are with Isfahan University of Technology, Isfahan, Iran. M. Shafie-khah is with School of Technology and Innovations, University of Vaasa, Vaasa 65200, Finland (e-mail: mshafiek@uwasa.fi).

$U_{g,t}$	Binary variable of commitment status for unit ***g***
$U_{g,t,\omega}$	Binary variable of commitment status for unit ***g*** at hour ***t*** at scenario ω
$U^{ch}_{e,t}, U^{dch}_{e,t}$	Binary variable related to charging /discharging status of battery ***e*** at hour ***t***
$S^{st}_{e,t}, S^{sd}_{e,t}$	Binary variable related startup /shutdown status of unit ***g*** at hour ***t***
$P^{dch}_{e,t}, P^{ch}_{e,t}$	Discharging/charging power of battery ***e***
$SOC_{e,t}$	State of charge of battery ***e*** at hour ***t***
$R^{Up}_{g,t,cl}, R^{Dn}_{g,t,cl}$	Scheduled up/downward active reserve power of unit ***g*** at hour ***t*** and control level ***cl***
$Q^{Up}_{g,t,cl}, Q^{Dn}_{g,t,cl}$	Scheduled up/downward reactive reserve power of unit ***g*** at hour ***t*** and control level ***cl***
$P^{+}_{b,b',t}, P^{-}_{b,b',t}$	Active power flow in up/down stream directions
$Q^{+}_{b,b',t}, Q^{-}_{b,b',t}$	Reactive power flow in up/down stream directions
$V2_{b,t}$	Auxiliary variable of squared voltage of bus ***b***
$I2_{b,b',t}$	Auxiliary variable of squared current of branch b,b' at hour ***t***
$\Delta f_{t,\omega,cl}$	Frequency excursion of MG in scenario ω at hour ***t*** and control level ***cl***
$r^{Up}_{g,t,\omega,cl}, r^{Dn}_{g,t,\omega,cl}$	Up/downward delivered active power deviation of unit ***g*** in scenario ω at hour ***t*** and control level ***cl***
$q^{Up}_{g,t,\omega,cl}, q^{Dn}_{g,t,\omega,cl}$	Up/downward delivered reactive power deviation of unit ***g*** in scenario ω at hour ***t*** and control level ***cl***
$f_{t,\omega,cl}$	MG's frequency in scenario ω at hour ***t*** and control level ***cl***

Definitions

$$\Delta X_{x,t,\omega,pri} = X_{x,t,\omega,pri} - X_{day-ahead}, \Delta X_{x,t,\omega,\sec} = X_{x,t,\omega,\sec} - X_{x,t,\omega,pri}$$

$$X \in \{P_{x,t,\omega,cl}, Q_{x,t,\omega,cl}, P_{x,t}, Q_{x,t}, P^{dch}_{e,t}, P^{ch}_{e,t}, P^{dch}_{e,t,\omega,cl}, P^{ch}_{e,t,\omega,cl},$$

$$P^{+}_{b,b',t}, P^{-}_{b,b',t}, Q^{+}_{b,b',t}, Q^{-}_{b,b',t}\}$$

I. Introduction

A. Aims & motivations

The last few decades have seen a growing popularity in developing microgrids (MGs) as a small-scale power system to integrate distributed energy resources (DER) [1]. Isolated MGs (IMG) lack of upstream network and suffer the system's low inertia, causing the MG's frequency being vulnerable to the variations of load demand and renewable energy resources (RES) generation [2]. Therefore, the secure operation of an IMG requires a proper energy management system to deal with voltage and frequency issues [3]. On the other hand, the desired model should guarantee the economic aspects of MG's operation and provide the condition for the presence of all prosumers.

According to [4], many off-grid remote communities worldwide meet their electricity demand from DERs in IMGs. The issue becomes more critical when the estimates from International Energy Agencies (IEA) show that 1.3 billion people around the world have no access to the existing grids but can potentially be supplied with IMGs that integrate local RES [5]. Considering the developments of IMGs and small-scale participants (prosumers) in those remote areas, the importance of energy trading in IMGs would be significant. Thus, the earlier reasons motivated us to propose a market-clearing model for IMGs. The purpose of the proposed model is to provide a mechanism for settling the energy market considering the operational challenges of IMGs.

B. Background & literature reviews

Energy management system (EMS) in IMGs is responsible for the economic and reliable operation considering optimal dispatch and schedules of DERs. The EMS strategies based on their access to the information can be classified as communication-based (e.g., centralized methods) and autonomous strategies [6]. In [7], a mixed-integer quadratic EMS is proposed considering active and reactive power balance and unbalanced system configuration for IMGs.

An optimal energy scheduling of a standalone MG, which considers the system's uncertainties to minimize operation and generated emission costs, is introduced in [8]. A two-stage decision process is represented by [9] and [10], but their optimization frameworks are different. In [9] authors implemented a robust approach, while a stochastic-predictive approach regarding MG's uncertainties is proposed in [10]. A unit-commitment and economic dispatch based on an improved genetic algorithm and MILP method for MGs are considered in [11]. An EMS based on techno-economic optimization that considers the energy life spans of DERs is proposed in[12]. In [4] and [13], a sustainable EMS model for IMGs is presented. In [4], equivalent emission functions and demand shifting loads are developed for DGs and included in an IMG EMS model. A nonlinear optimal predictive control algorithm that manages the batteries' energy and load-shedding strategies is presented in [13] to balance the load and generation in an IMG. In [14], a nonlinear probabilistic EMS with reduced unscented transformation is applied to deal with uncertain market price values and RES output power. Furthermore, AC network constraints and the correlation between market price and load demand are considered in [14]. A risk-based reverse decision approach for optimal day-ahead scheduling of IMGs is presented in [15]. Besides the correlation of input variables, a multi-type reserve scheme is considered according to the different operational conditions of DERs in [15]. In [16], an EMS model based on three different operational strategies of diesel engine generators is studied. The proposed model in [16] is nonlinear, and an artificial bee colony is utilized to achieve the goals.

As the above literature shows, some proposed models are nonlinear and cannot guarantee the optimality of schedules. Also, frequency security constraints as a crucial part of secure operation in IMGs are neglected in papers earlier examined. The frequency control mechanism is an essential need for IMGs ignoring this issue can severely decrease the operation reliability [17]. In [17],[2], and [1], some methods for frequency control in IMGs are offered, but only a few works in this literature have included the frequency issues of IMGs in EMS models. In [3], a nonlinear EMS model considers short-term fluctuations and their effects on frequency and operation. A stochastic gain adaptive EMS model is proposed in [18] to provide a secure frequency control portfolio. However, in these studies, the hierarchical structure, reserves management and the AC network constraints are not considered.

C. Micro-Market & its necessity

In recent years, the integration of DERs has led to fundamental changes in the power system structure, so the DER's power variations can be matched with local demand variations and provide a local trading system [19]. On the other hand, current wholesale electricity markets cannot respond to intermittency stems from load and DERs in real-time. Moreover, the market prices will usually be determined on a national level that cannot

mirror the energy surplus or shortage of supply. MG's energy markets are a solution to provide a sustainable, reliable, and local balance of generation and consumption economically and allow prosumers to trade in an MG actively [20]. A Micro-Market (μM) is an EMS based on market rules that manages the MG's DERs to maximize their time of use and is responsible for providing energy and flexibility services. In general, the μM tries to develop local trading to encourage the local generation and prosumers participation for maximizing MG's profits [19].

According to [19]-[21], the μM advantages can be summarized as follows:

- The μM provides a platform for small-scale participants (prosumers and consumers) to trade locally generated power in their community. Therefore, it develops the local energy consumption close to its generation and provides efficient use of local resources and sustainability.
- The μM will decrease the cost of energy transportation and power losses by supplying demand through local resources.
- The μM reduces the latency of congestion management and distribution faults.
- The μM enhances the self-sufficiency in MG's community and increases the possibility of cost reduction.
- The μM keeps the profits in MG's community through local transactions and encourages market participants to reinvestment in RESs.
- The μM strengthen the trade of end-user flexibility for the MG's benefit.

To the best of our knowledge, there are few papers with the market-based approach in MGs.In [22], an EMS model for building MGs considering batteries as a flexibility source is proposed. The nonlinear EMS model also considers the battery degradation and real-life operation using a market-based setting. A decentralized market model regarding carbon emission rights is proposed in [23]. The market model in [23] economically uses energy storages for power balance, and a tracker-based distributed algorithm is presented for some local constraints. In [24] and [25], nonlinear EMS models with electricity pricing are proposed. In [24], a stochastic nodal price-based scheduling considering uncertainties of RES and electricity pricing is developed. An optimization scheme to minimize the electricity price in an MG by providing a scheme for energy trading is presented in [25]. In [22]-[24], the hierarchical structure of MGs, frequency security, and active-reactive reserve management are not considered.

C. Contributions and paper structure

Upon reviewing previous studies, it can be seen that that the traditional electricity market models cannot deal with the operational challenges of IMGs. Also, a framework for energy trading that considers both the demand and supply side while the secure operation of IMGs is ensured needs to be provided by the current energy management models. In addition, pricing mechanism, data privacy, resource efficiency, business models and future contracts are other difficulties of market based approaches [26],[19]. As the literature showed, most of the previous works mainly have focused only on active power scheduling, and reactive power scheduling is not considered. Also, the joint active-reactive reserve scheduling of isolated microgrids, which guarantees the system's secure operation and frequency security, has yet to be considered. The secure operation and economic goals of the IMG could achieve through a proper control structure. However, the studies do not model the hierarchical control structure and the operational uncertainties simultaneously. In order to fill the mentioned research gap, this paper proposes a two-stage MILP μM model considering hierarchical control levels and guarantees globally optimal results. The following are the main contributions of this study:

- The proposed μM model develops a framework for local electricity trading in an isolated microgrid that guarantees global optimal results. Since the proposed model utilized a bidirectional linearized AC power flow, the condition for energy exchange is provided for prosumers, and the necessity of reactive power in isolated microgrids is also well addressed. The proposed stochastic model not only considers the joint active-reactive power scheduling but also the uncertainties of load demand, wind speed, and solar radiation are taken into account by scheduling sufficient active-reactive power reserves.
- The uncertainty of load and renewable energy resources, besides the lack of an upstream network and the isolated microgrid's low inertia, put the microgrid's frequency at risk. To ensure the secure operation of the isolated microgrid, this paper models the hierarchical control levels, including both primary and secondary levels, for the first time in a market environment. Unlike existing literature, the DGs' droop controllers, frequency security constraints and voltage limits are simultaneously modeled in both primary and secondary control levels.

The rest of this paper is organized as follows: Section II describes the proposed μM and the problem formulation. The reports and result discussions are provided in Section III. Finally, the conclusion is available in Section IV.

II. FORMULATION

This section will explain the problem formulation in four main parts. In the first subsection, the objective function of the μM is introduced in four parts. Then based on the proposed model's different time stages, the constraints of the problem are mentioned, and the linearization method is described in the last part.

The proposed μM aims to maximize social welfare (SW) through the optimal scheduling of active-reactive power and reserve for the next day. This goal is more challenging in IMGs where operational uncertainties put the IMG's frequency security at risk. In order to keep the IMG's frequency in a pre-defined range and provide a local trading framework, a centralized two-stage stochastic μM model is introduced in this paper. In the first stage, some decisions (e.g., commitment and set-points of controllable DGs, accepted demand load, primary and secondary reserve) are made a day before the operation. However, in the second stage, other decision variables (e.g., delivered active-reactive power deviation in primary and secondary control level, demand response) are determined throughout scenarios to compensate for any unpleasant effect resulting from the first-stage decision.

This paper considers that transient modes are cleared, and the IMG's frequency excursions are fixed into the steady state as the hourly frequency. Also, this paper assumes that all the DGs offer their generated active power based on their marginal costs and that there is no collusion among different μM participants. The customers (prosumers) can participate in the μM

independently or aggregators accumulates flexibility from different participants (especially prosumers) to sell it to μM [27]. Also, it is assumed that microgrid system operator (MSO) has adopted the market role as the trusted third party (TTP) and organizes the μM. ESSs are owned by the MSO and are only used to perform flexibility services such as load time shifting, so their offers and bids for charging and discharging are considered zero. The uniform pricing method is used in the proposed μM, and active generated power at each bus is priced using the locational marginal pricing (LMP) method. The following parts describe the mathematical formulation of the proposed model.

A. Objective function

In a market environment efficiency includes both supply and demand side and the market is efficient when SW is maximized. The Social Welfare will be defined as the sum of net consumers' surplus and of the producers' profit and it quantifies the overall benefit that arises from trading [28]. The objective function of the proposed μM, which consists of four parts, is fully discussed below. The first part considers the SW at the day-ahead stage.

$$OF_1 = \sum_{t=1}^{N_T}\sum_{l=1}^{N_L} C_{l,t}^{P} P_{l,t} - \sum_{t=1}^{N_T}\sum_{g=1}^{N_G} C_{g,t}^{P} P_{g,t} - \sum_{t=1}^{N_T}\sum_{w=1}^{N_W} C_{w,t}^{P} P_{w,t} - \sum_{t=1}^{N_T}\sum_{s=1}^{N_S} C_{s,t}^{P} P_{s,t} \quad (1)$$

In (1), the first term represents the consumers' profit and the second to fourth terms indicate the profit of other μM participants including diesel generators, wind turbines, and solar units. Since the primary interval in comparison to the scheduling horizon is too short (a few seconds in comparison to hour), the equations of this control level are not considered in the objective function. Like (1), Eq. (2) includes the expected SW at the balancing stage in the secondary control level. Therefore, the first term is the consumer's profit difference between the balancing stage and day-ahead stage in the secondary interval. Subsequently, the second to fourth terms represent the producers' profit difference between the mentioned stages in the secondary interval. The last term also shows the demand response term at this control level.

$$OF_2 = \sum_{\omega=1}^{N_\omega} \pi_\omega \left\{ \begin{array}{l} \sum_{t=1}^{N_T}\sum_{L=1}^{N_L} C_{l,t}^{P} \left(P_{l,t,\omega,\text{sec}} - P_{l,t} \right) \\ -\sum_{t=1}^{N_T}\sum_{g=1}^{N_G}\sum_{cl} C_{g,t}^{P} \left(r_{g,t,\omega,cl}^{Up} - r_{g,t,\omega,cl}^{Dn} \right) \\ -\sum_{t=1}^{N_T}\sum_{w=1}^{N_W} C_{w,t}^{P} \left(P_{w,t,\omega,\text{sec}} - P_{w,t} \right) \\ -\sum_{t=1}^{N_T}\sum_{s=1}^{N_S} C_{s,t}^{P} \left(P_{s,t,\omega,\text{sec}} - P_{s,t} \right) \\ -\sum_{t=1}^{N_T}\sum_{d=1}^{N_D} C_{d,t}^{P} \left(P_{d,t,\omega,\text{sec}} \right) \end{array} \right\} \quad (2)$$

The start-up and shut-down costs are expressed in the first part of (3). The second terms indicate the upward and downward active reserve provision cost for both primary and secondary intervals. Like the second terms, the last term is dedicated to reactive reserve provision costs.

$$OF_3 = \left(\sum_{t=1}^{T}\sum_{G=1}^{N_G} C_g^{St} S_{G,t}^{st} + \sum_{t=1}^{T}\sum_{G=1}^{N_G} C_g^{Sd} S_{G,t}^{sd} \right) + \left(\sum_{t=1}^{T}\sum_{g=1}^{N_G}\sum_{cl} C_{g,t,cl}^{R,P} \left(R_{g,t,cl}^{Up} + R_{g,t,cl}^{Dn} \right) \right) + \left(\sum_{t=1}^{T}\sum_{g=1}^{N_G}\sum_{cl} C_{g,t,cl}^{R,Q} \left(Q_{g,t,cl}^{Up} + Q_{g,t,cl}^{Dn} \right) \right) \quad (3)$$

The last part of the objective function that is responsible for minimizing frequency deviations is formulated as follows:

$$OF_4 = \sum_{\omega=1}^{N_\omega} \pi_\omega \left(\frac{1}{f_{ref}} \sum_{t=1}^{T}\sum_{cl} \left| f_{t,\omega,cl} - f_{ref} \right| \right) \quad (4)$$

The complete objective function of μM is presented in (5).

$$OF = \sum_{i=1}^{2} OF_i - \sum_{i=3}^{4} OF_i \quad (5)$$

B. Day-Ahead stage constraints

In order to ensure the secure operation of the IMG, the μM should consider several operational constraints which are presented in following subsections. In this stage, the active-reactive power and the active-reactive regulation reserve of each generating unit, will determine. In addition, the accepted load demand of each consumer, will be obtained in this stage. Consideration of the following constraints is necessary for this stage.

Linearized AC power flow

Applying an AC power flow makes the μM model more comprehensive, but it will lead to nonlinear terms. On the other hand, concerning the presence of prosumers in μM, it is necessary to implement a bidirectional power flow. To fix the mentioned issues, in this paper, a bidirectional linearized AC power flow based on [29] is taken into account.

$$V2_{b,t} - V2_{b',t} - Z_{b,b'}^{2} I2_{b,b',t} - 2R_{b,b'} \left(P_{b,b',t}^{+} - P_{b,b',t}^{-} \right) - 2X_{b,b'} \left(Q_{b,b',t}^{+} - Q_{b,b',t}^{-} \right) = 0 \quad (6)$$

$$V2_{Rated,b} I2_{b,b',t} = \sum_{f} \left[(2f-1) \Delta S_{b,b'} \Delta P_{b,b',f,t} \right] + \sum_{f} \left[(2f-1) \Delta S_{b,b'} \Delta Q_{b,b',f,t} \right] \quad (7)$$

$$0 \le \left(Q_{b,b',t}^{+} + Q_{b',b,t}^{-} \right) \le V_{Rated} \times I_{\max,b,b'} \quad (8)$$

$$0 \le \left(P_{b,b',t}^{+} + P_{b',b,t}^{-} \right) \le V_{Rated} \times I_{\max,b,b'} \quad (9)$$

$$P_{b,b',t}^{+} + P_{b',b,t}^{-} = \sum_{f} \Delta P_{b,b',f,t} \quad (10)$$

$$Q_{b,b',t}^{+} + Q_{b',b,t}^{-} = \sum_{f} \Delta Q_{b,b',f,t} \quad (11)$$

$$0 \le \Delta P_{b,b',f,t} \le \Delta S_{b,b'} \quad (12)$$

$$0 \le \Delta Q_{b,b',f,t} \le \Delta S_{b,b'} \quad (13)$$

$$\Delta S_{b,b'} = \frac{V_{Rated} \times I_{\max,b,b'}}{F} \quad (14)$$

$$V_{\min} \le V2_{b,t} \le V_{\max} \quad (15)$$

Eq. (6) shows the voltage balance between two buses. It should be noted that *V2* is an auxiliary variable to represent the squared voltage relation. Eq. (7) is implemented to linearize the active and reactive power flows, and inequalities (8)-(9) consider the maximum apparent power limits. Finally, Eq.(10)-(15) are employed for piecewise linearization and voltage limits constraint.

Active and reactive power balance

To ensure the active power balance for each MG's bus and at each hour of time horizon Eq. (16) is implemented. The first term on the left of Eq.(16) shows the power generated by the various units, and the next terms include the lines' power flow. Assuming that wind and solar units operate under the predefined power factor, Eq. (17) shows a similar form of reactive power balance.

$$\left(\sum_{g\in N_b^G} P_{g,t} + \sum_{w\in N_b^W} P_{w,t} + \sum_{s\in N_b^S} P_{s,t} + \sum_{e\in N_b^E} P_{e,t}^{dch}\right) - \sum_{b'}\left[\left(P_{b,b',t}^{+} - P_{b,b',t}^{-}\right) + R_{b,b'} I2_{b,b',t}\right] + \sum_{b'}\left(P_{b',b,t}^{+} - P_{b',b,t}^{-}\right) = \sum_{l\in N_b^L} P_{l,t} + \sum_{l\in N_b^E} P_{e,t}^{ch} \quad \forall b\in B, \forall t\in T \tag{16}$$

$$\sum_{g\in N_b^G} Q_{g,t} + \sum_{w\in N_b^W} Q_{w,t} + \sum_{s\in N_b^S} Q_{s,t} + \sum_{b'}\left(Q_{b',b,t}^{+} - Q_{b',b,t}^{-}\right) - \sum_{b'}\left[\left(Q_{b,b',t}^{+} - Q_{b,b',t}^{-}\right) + X_{b,b'} I2_{b,b',t}\right] = \sum_{l\in N_b^L} Q_{l,t} \quad \forall b\in B, \forall t\in T \tag{17}$$

ESS constraints

The relevant operational constraints of batteries, are presented in (18)-(22), and Eq. (23) guarantees that batteries cannot charge or discharge simultaneously [7].

$$SOC_{e,t} = SOC_{e,t-1} + \left(P_{e,t}^{ch}\eta_e^{ch} - \frac{P_{e,t}^{dch}}{\eta_e^{dch}}\right)\Delta t \quad \forall e\in E, \forall t\neq 1, t\in T \tag{18}$$

$$SOC_e^{Min} \le SOC_{e,t} \le SOC_e^{Max} \quad \forall e\in E, \forall t\in T \tag{19}$$

$$0 \le P_{e,t}^{ch} \le U_{e,t}^{ch} P_e^{Max,ch} \quad \forall e\in E, \forall t\in T \tag{20}$$

$$0 \le P_{e,t}^{dch} \le U_{e,t}^{dch} P_e^{Max,dch} \quad \forall e\in E, \forall t\in T \tag{21}$$

$$SOC_{e,23} = SOC_{e,0} \quad \forall e\in E \tag{22}$$

$$U_{e,t}^{dch} + U_{e,t}^{ch} \le 1 \quad \forall e\in E, \forall t\in T \tag{23}$$

Generating Units constraints

According to the hierarchical control levels in an IMG, the DGs' primary and secondary reserves are restricted in (24)-(27). The commitment binary variable $U_{g,t}$ on the right side of (25) and (27), guarantees that this constraint is not violated by P_g^{Min} when the unit is not committed at the day-ahead stage. Unlike the (25) and (27), due to the ability of changing unit commitment using fast start capability in the secondary level, the commitment binary variable of the day-ahead stage is avoided in constraints (24) and (26). The absence of $U_{g,t}$ in the mentioned constraints causes the secondary control level to add fast start units at the second stage independent of the primary control level.

$$P_{g,t} + R_{g,t,pri}^{Up} + R_{g,t,\sec}^{Up} \le P_g^{Max} \quad \forall g\in G, \forall t\in T \tag{24}$$

$$P_{g,t} - R_{g,t,pri}^{Dn} - R_{g,t,\sec}^{Dn} \ge P_g^{Min} U_{g,t} \quad \forall g\in G, \forall t\in T \tag{25}$$

$$Q_{g,t} + Q_{g,t,pri}^{Up} + Q_{g,t,\sec}^{Up} \le Q_g^{Max} \quad \forall g\in G, \forall t\in T \tag{26}$$

$$Q_{g,t} - Q_{g,t,pri}^{Dn} - Q_{g,t,\sec}^{Dn} \ge Q_g^{Min} U_{g,t} \quad \forall g\in G, \forall t\in T \tag{27}$$

Eq. (28)-(46) ensure that the technical constraints of different generating units are included. Eq. (28)-(29) considers the ramp-up and ramp-down rates of generators, and the start-up and shut-down constraints of generators are modeled by (30)-(31) [30]. The active and reactive output power of diesel generators are restricted by (32) and (33). In (34)-(37), the scheduled active and reactive power of RES is limited to their available generation. Inequality (38) shows the range of active load demand and subsequently the reactive load demand will determine depending on the load power factor in (39) [30] , [31].

$$P_{g,t} - P_{g,t+1} \le R_g^{Dn} + S_{g,t}^{sd} P_g^{Min} \quad \forall g\in G, \forall t\in T \tag{28}$$

$$P_{g,t+1} - P_{g,t} \le R_g^{Up} + S_{g,t}^{st} P_g^{Min} \quad \forall g\in G, \forall t\in T \tag{29}$$

$$S_{g,t}^{st} - S_{g,t}^{sd} = U_{g,t} - U_{g,t-1} \quad \forall g\in G, \forall t\in T \tag{30}$$

$$S_{g,t}^{st} + S_{g,t}^{sd} \le 1 \quad \forall g\in G, \forall t\in T \tag{31}$$

$$U_{g,t} P_g^{Min,} \le P_{g,t} \le U_{g,t} P_g^{Max} \quad \forall g\in G, \forall t\in T \tag{32}$$

$$U_{g,t} Q_g^{Min,} \le Q_{g,t} \le U_{g,t} Q_g^{Max} \quad \forall g\in G, \forall t\in T \tag{33}$$

$$0 \le P_{s,t} \le \alpha_{s,t} P_s^{Max} \quad \forall s\in S, \forall t\in T \tag{34}$$

$$-\alpha_{s,t} Q_s^{Min} \le Q_{s,t} \le \alpha_{s,t} Q_s^{Max} \quad \forall s\in S, \forall t\in T \tag{35}$$

$$0 \le P_{w,t} \le \alpha_{w,t} P_w^{Max} \quad \forall w\in W, \forall t\in T \tag{36}$$

$$-\alpha_{w,t} Q_w^{Min} \le Q_{w,t} \le \alpha_{w,t} Q_w^{Max} \quad \forall w\in W, \forall t\in T \tag{37}$$

$$0 \le P_{l,t} \le \alpha_{l,t} P_l^{Max} \quad \forall l\in L, \forall t\in T \tag{38}$$

$$Q_{l,t} = P_{l,t} \tan(\varphi_l) \quad \forall l\in L, \forall t\in T \tag{39}$$

Also, Eq. (40)- (46), represent the linear form of minimum uptime and downtime of DGs [30] .

$$\sum_{t=1}^{\zeta_g} 1 - U_{g,t} = 0 \quad \forall g, \forall t \tag{40}$$

$$\sum_{t=k}^{k+T_g^{Up}-1} U_{g,t} \ge T_g^{Up} S_{g,t}^{st} \quad \forall g, \forall t \quad \forall k = \zeta_g + 1..T - T_g^{Up} + 1 \tag{41}$$

$$\zeta_g = \min\left\{T, \left(T_g^{Up} - U_0\right) U_{g,0}\right\} \tag{42}$$

$$\sum_{t=1}^{\zeta_g} U_{g,t} = 0 \quad \forall g, \forall t \tag{43}$$

$$\sum_{t=k}^{k+T_g^{Dn}-1} 1 - U_{g,t} \ge T_g^{Dn} S_{g,t}^{sd} \quad \forall k = \zeta_g + 1 \ \ldots \ T - T_g^{Dn} + 1 \tag{44}$$

$$\sum_{t=k}^{T} \left(1 - U_{g,t} - S_{g,t}^{sd}\right) \ge 0 \quad \forall k = T - T_g^{Dn} + 2 \ \ldots \ T \tag{45}$$

$$\zeta_g = \min\left\{T, \left(T_g^{Dn} - S_0\right)(1 - U_{g,0})\right\} \tag{46}$$

C. Balancing stage and hierarchical control levels

At this stage due to operational uncertainties, the scheduled active-reactive power of different μM participants, is readjusted. Also, the reserve power of DGs based on their droop controller characteristics and network frequency security constraints could be rescheduled. The hierarchical control levels at this stage are formulated as follows:

Primary frequency excursion

In an IMG, due to the lack of an upstream network, it is essential to consider corrective control actions for voltage and frequency restoration. In the hierarchical control structure, providing an adequate amount of primary reserve, which can be developed in a few seconds, plays a crucial role in keeping the frequency in a safe range. According to the power balance in the MG's network, the primary frequency excursion could be described as follows:

$$\begin{aligned}&\sum_{g=1}^{N_G}\Delta P_{t,\omega,pri}=\sum_{g=1}^{N_G}\left(P_{g,t,\omega,pri}-P_{g,t}\right)=\sum_{g=1}^{N_G}\left(r_{g,t,\omega,pri}^{Up}-r_{g,t,\omega,pri}^{Dn}\right)\\&=\sum_{l=1}^{N_L}\left(P_{l,t,\omega,pri}-P_{l,t}\right)+\sum_{e=1}^{N_E}\left(P_{e,t,\omega,pri}^{ch}-P_{e,t}^{ch}\right)+\\&\sum_{l=1}^{N_l}\left(P_{pri}^{loss}-P^{loss}\right)-\sum_{w=1}^{N_W}\left(P_{w,t,\omega,pri}-P_{w,t}\right)\\&-\sum_{s=1}^{N_S}\left(P_{s,t,\omega,pri}-P_{s,t}\right)-\sum_{s=1}^{N_E}\left(P_{e,t,\omega,pri}^{dch}-P_{e,t}^{dch}\right)\end{aligned}\tag{47}$$

Medium-voltage IMGs use high-capacity feeders, which are thicker and have higher X/R ratios compared to low-voltage MGs [7]. Since this paper proposes the μM for medium-voltage IMGs, the steady state power-frequency relation of droop based DGs could be described as follows [32]:

$$r_g\left(\Delta P_{g,t,\omega,pri}-\Delta P_{g,t,\omega,pri}^{ref}\right)=U_{g,t}\left(\Delta f_{t,\omega,pri}^{ref}-\Delta f_{t,\omega,pri}\right)\tag{48}$$

Note that the droops gains are considered as constant parameters in Eq. (49) and they don't change during operating horizon. Since the primary control level has the fastest time response, there is no time to change the reference value or the commitment of DGs. Therefore, these variables are constant during primary level and equal to the Day-Ahead stage:

$$\Delta f_{t,\omega,pri}^{ref}=0\tag{50}$$

$$\Delta P_{g,t,\omega,pri}^{ref}=0\tag{51}$$

Thus, considering the (48) and substituting (47) into (48), the frequency excursion in the primary level describes as follows:

$$\Delta f_{t,\omega,pri}=\frac{-\sum_{g=1}^{N_G}\left(r_{g,t,\omega,pri}^{Up}-r_{g,t,\omega,pri}^{Dn}\right)}{\sum_{g=1}^{N_G}\left(\frac{U_{g,t}}{r_g}\right)}\tag{52}$$

$$\Delta f_{t,\omega,pri}=f_{t,w,pri}-f_0\tag{53}$$

$$\left|\Delta f_{t,\omega,pri}\right|\le\Delta f_{pri}^{Max}\tag{54}$$

Primary active and reactive reserve

To compensate for the primary frequency excursion and keep the frequency in the desired range, DGs should be able to increase or decrease their output power. Depending on imbalances that occurs in the IMG and frequency safe bound, the allocated primary reserves are determined as follows:

$$0\le r_{g,t,\omega,pri}^{Up}-r_{g,t,\omega,pri}^{Dn}\le R_{g,t,pri}^{Up}\le R_{g,t}^{Up_{Max}}U_{g,t}\quad\forall g\in G,t\in T,\omega\in\Omega\tag{55}$$

$$0\le r_{g,t,\omega,pri}^{Dn}-r_{g,t,\omega,pri}^{Up}\le R_{g,t,pri}^{Dn}\le R_{g,t}^{Dn_{Max}}U_{g,t}\quad\forall g\in G,t\in T,\omega\in\Omega\tag{56}$$

$$0\le q_{g,t,\omega,pri}^{Up}-q_{g,t,\omega,pri}^{Dn}\le Q_{g,t,pri}^{Up}\le Q_{g,t}^{Up_{Max}}U_{g,t}\quad\forall g\in G,t\in T,\omega\in\Omega\tag{57}$$

$$0\le q_{g,t,\omega,pri}^{Dn}-q_{g,t,\omega,pri}^{Up}\le Q_{g,t,pri}^{Dn}\le Q_{g,t}^{Dn_{Max}}U_{g,t}\quad\forall g\in G,t\in T,\omega\in\Omega\tag{58}$$

$$P_g^{Min}U_{g,t}\le P_{g,t}+r_{g,t,\omega,pri}^{Up}-r_{g,t,\omega,pri}^{Dn}\le P_g^{Max}U_{g,t}\quad\forall g\in G,t\in T,\omega\in\Omega\tag{59}$$

$$Q_g^{Min}U_{g,t}\le Q_{g,t}+q_{g,t,w,pri}^{Up}-q_{g,t,w,pri}^{Dn}\le Q_g^{Max}U_{g,t}\quad\forall g\in G,t\in T,\omega\in\Omega\tag{60}$$

Eq. (55)-(58), ensure that the active and reactive delivered power deviations will not exceed the amount of reserve allocated to each unit. Also, (59) and (60) guarantee that primary active and reactive power are restricted by their limits.

Secondary frequency excursion

Since the secondary control level has a lower time response, it would be able to move power set points of dispatchable units to guarantee the secure operation of the IMG. Also, in this control level, the μM is capable of utilizing the fast start ability to help the dispatched units keep the secondary frequency in the predefined range. The following equations describe its performance:

$$\sum_{g=1}^{N_G}\Delta P_{t,\omega,\sec}=\sum_{g=1}^{N_G}\left(P_{g,t,\omega,\sec}-P_{g,t,\omega,pri}\right)=\sum_{g=1}^{N_G}\left(r_{g,t,\omega,\sec}^{Up}-r_{g,t,\omega,\sec}^{Dn}\right)\tag{61}$$

The delivered power deviation between primary and secondary control levels with is shown with $r_{g,t,\omega,sec}^{Dn}$ and $r_{g,t,\omega,sec}^{Up}$. Therefore, the secondary frequency excursion regard to (47), (48), and (61) will be obtained:

$$\Delta f_{t,\omega,\sec}=\frac{\sum_{g=1}^{N_G}\left(P_{g,t,\omega,\sec}^{ref}-P_{g,t,\omega,\sec}\right)}{\sum_{g=1}^{N_G}\frac{U_{g,t,\omega}}{r_g}}=\frac{\sum_{g=1}^{N_G}\left(P_{g,t,\omega,\sec}^{ref}-\left(\sum_{cl}(r_{g,t,\omega,cl}^{Up}-r_{g,t,\omega,cl}^{Dn})+P_{g,t}\right)\right)}{\sum_{g=1}^{N_G}\frac{U_{g,t,\omega}}{r_g}}\tag{62, 63}$$

$$\Delta f_{t,\omega,\sec}=f_{t,\omega,\sec}-f_0\tag{64}$$

$$\left|\Delta f_{t,\omega,\sec}\right|\le\Delta f_{\sec}^{Max}\tag{65}$$

Secondary active and reactive reserve

As it is clear from (62) and (66)-(71), the secondary control level, in comparison to the primary control level, has more abilities to control frequency excursion. The first advantage is the ability to change the power set points, which is modeled by $P_{g,t,\omega,\sec}^{ref}$. In addition, this control level can utilize the fast start

capability of DGs to add new units for secondary reserve which is modeled the binary variable $U_{g,t,\omega}$.

$$0 \le r^{Up}_{g,t,\omega,\sec} - r^{Dn}_{g,t,\omega,\sec} \le R^{Up}_{g,t,\sec} \le R^{Up_{Max}}_{g,t} U_{g,t,\omega} \quad \forall g \in G, t \in T, \omega \in \Omega \tag{66}$$

$$0 \le r^{Dn}_{g,t,\omega,pri} - r^{Up}_{g,t,\omega,\sec} \le R^{Dn}_{g,t,\sec} \le R^{Dn_{Max}}_{g,t} U_{g,t,\omega} \quad \forall g \in G, t \in T, \omega \in \Omega \tag{67}$$

$$0 \le q^{Up}_{g,t,\omega,\sec} - q^{Dn}_{g,t,\omega,\sec} \le Q^{Up}_{g,t,\sec} \le Q^{Up_{Max}}_{g,t} U_{g,t,\omega} \quad \forall g \in G, t \in T, \omega \in \Omega \tag{68}$$

$$0 \le q^{Dn}_{g,t,\omega,\sec} - q^{Up}_{g,t,\omega,\sec} \le Q^{Dn}_{g,t,\sec} \le Q^{Dn_{Max}}_{g,t} U_{g,t,\omega} \quad \forall g \in G, t \in T, \omega \in \Omega \tag{69}$$

$$P^{Min}_{g} U_{g,t,\omega} \le P_{g,t} + \sum_{cl} (r^{Up}_{g,t,w,cl} - r^{Dn}_{g,t,w,cl}) \le P^{Max}_{g} U_{g,t,\omega} \quad \forall g \in G, t \in T, \omega \in \Omega \tag{70}$$

$$Q^{Min}_{g} U_{g,t,\omega} \le Q_{g,t} + \sum_{cl} (q^{Up}_{g,t,w,cl} - q^{Dn}_{g,t,w,cl}) \le Q^{Max}_{g} U_{g,t,\omega} \quad \forall g \in G, t \in T, \omega \in \Omega \tag{71}$$

$$P^{Min}_{g} U_{g,t,\omega} \le P^{ref}_{g,t,\omega.\sec} \le P^{Max}_{g} U_{g,t,\omega} \quad \forall g \in G, t \in T, \omega \in \Omega \tag{72}$$

$$P^{ref}_{g,t,\omega.\sec} - P_{g,t} \le R^{Up}_{g,t,\sec} \quad \forall g \in G, t \in T, \omega \in \Omega \tag{73}$$

$$P_{g,t} - P^{ref}_{g,t,\omega.\sec} \le R^{Dn}_{g,t,\sec} \quad \forall g \in G, t \in T, \omega \in \Omega \tag{74}$$

Similar to the primary level, inequalities (66)-(69) indicate the secondary delivered power deviations limits and the secondary active-reactive power is restricted by (70) and (71). In addition to previous constraints, inequalities (72)-(74) ensure that $P^{ref}_{g,t,\omega,\sec}$ will not exceed its limits.

Power balance and other second stage constraints

It should be mentioned that besides all constraints related to linearized ac power flow and energy storage, the following constraints should be considered in the second stage:

$$\begin{aligned} &\sum_{g \in N^G_b} \left(r^{Up}_{g,t,\omega,cl} - r^{Dn}_{g,t,\omega,cl}\right) + \sum_{w \in N^W_b} \left(\Delta P_{w,t,\omega,cl}\right) + \sum_{s \in N^S_b} \left(\Delta P_{s,t,\omega,cl}\right) \\ &+ \sum_{e \in N^E_b} \left(\Delta P^{dch}_{e,t,\omega,cl}\right) + \sum_{b'} \left(\Delta P^{+}_{b',b,t,\omega,cl} - \Delta P^{-}_{b',b,t,\omega,cl}\right) \\ &- \sum_{b'} \left(\left(\Delta P^{+}_{b,b',t,\omega,cl} - \Delta P^{-}_{b,b',t,\omega,cl}\right) + \Delta P^{loss}_{cl}\right) \\ &= \sum_{l \in N^L_b} \left(\Delta P_{l,t,\omega,cl}\right) + \sum_{e \in N^E_b} \left(\Delta P^{ch}_{e,t,\omega,cl}\right) - \sum_{d \in N^D_b} P_{d,t,\omega,cl} \\ &\forall b \in B, \forall t \in T, \forall \omega \in \Omega, \forall cl \in CL \end{aligned} \tag{75}$$

Eq. (75) represents the active power balance at the second stage in both the primary and secondary control level. This equation guarantees that the power difference between the day-ahead stage and the balancing stage in the primary control level will be supplied by the primary delivered power deviation that will lead to primary reserve. Also, Eq. (75) includes the power balance in the secondary control level and ensures that the secondary reserve will meet the power difference between the primary and the secondary control level at the second stage. Similarly, Eq. (76) guarantees reactive power balance for each MG's bus at both control levels. Inequalities (77)-(80) convey that the active and reactive power of RESs in each scenario is limited to their available generation.

$$\begin{aligned} &\sum_{g \in N^G_b} \left(q^{Up}_{g,t,\omega,cl} - q^{Dn}_{g,t,\omega,cl}\right) + \sum_{w \in N^W_b} \left(\Delta Q_{w,t,\omega,cl}\right) + \sum_{s \in N^S_b} \left(\Delta Q_{s,t,\omega,cl}\right) \\ &+ \sum_{b'} \left(\Delta Q^{+}_{b',b,t,\omega,cl} - \Delta Q^{-}_{b',b,t,\omega,cl}\right) \\ &- \sum_{b'} \left(\left(\Delta Q^{+}_{b,b',t,\omega,cl} - \Delta Q^{-}_{b,b',t,\omega,cl}\right) + \Delta P^{loss}_{cl}\right) = \sum_{l \in N^L_b} \left(\Delta Q_{l,t,\omega,cl}\right) \\ &- \sum_{d \in N^D_b} Q_{d,t,\omega,cl} \quad \forall b \in B, \forall t \in T, \forall \omega \in \Omega, \forall cl \in CL \end{aligned} \tag{76}$$

$$0 \le P_{s,t,\omega,cl} \le \alpha_{S,t,\omega} P^{Max}_{S} \quad \forall s \in S, \forall t \in T, \forall \omega \in \Omega, \forall cl \in CL \tag{77}$$

$$-\alpha_{S,t,\omega} Q^{Max}_{S} \le Q_{s,t,\omega,cl} \le \alpha_{S,t,\omega} Q^{Max}_{S} \quad \forall s \in S, \forall t \in T, \forall \omega \in \Omega, \forall cl \in CL \tag{78}$$

$$0 \le P_{w,t,\omega,cl} \le \alpha_{w,t,\omega} \quad P^{Max}_{w} \quad \forall s \in S, \forall t \in T, \forall \omega \in \Omega, \forall cl \in CL \tag{79}$$

$$-\alpha_{w,t,\omega} Q^{Max}_{w} \le Q_{w,t,\omega,cl} \le \alpha_{S,t,\omega} Q^{Max}_{w} \quad \forall s \in S, \forall t \in T, \forall \omega \in \Omega, \forall cl \in CL \tag{80}$$

D. Linearization method

In order to provide a MILP form of μM, the nonlinear terms in (4), (52), and (62) are linearized using the methods which are available in study [33].

III. Results and Discussions

In this section, the simulation results of the proposed model are discussed. First, the test system and solution algorithm are introduced, and then the simulation results are analyzed and compared in different time intervals.

A. Test system and solution algorithm

The proposed μM model for IMGs is evaluated on the modified CIGRE network presented in [7]. The total generation capacity of the test system, including all DERs, is equal to 9216 kW. The lines, loads, and all DER parameters are identical to the study in [7]. The introduced μM model considers all uncertainties of load, wind speed, and solar irradiations for the operating horizon, and the results will derive for the next day with hourly time step. In the first step, historical data of uncertain parameters are defined as inputs for the scenario generation module. In this module, based on what is studied in [34], 343 scenarios with the probability of each scenario are generated. Since considering this number of scenarios leads to more challenging problem solving, the size of scenarios is reduced to 14 using the SCENERD tool in GAMS software. Then, the load demand and available output power of renewable resources in each scenario with its probability are determined as the outputs of the scenario generating module. In the next step, the outputs of the scenario generating module beside the isolated microgrid's network information (information like network topology, the capacity of lines, resistance and reactance of lines) and μM participants' data, including their bids and offers, generation and reserve capacity and droop characteristics are defined as the inputs of μM model. In the final step, the proposed μM model is solved, and the results, including the active-reactive power schedule, active-reactive reserve schedule, the LMPs, frequency deviations, and other needed variables, will be obtained for the next 24 hours.

B. Simulation results

The proposed MILP model that ensures the globally optimal solutions is coded in high-level optimization modeling

language GAMS. The computation time for 0.5% relative gap is about 742 seconds and for 0.05% relative gap is close to three hours. The µM model introduced in this paper was solved using GUROBI 7.0.1 on a 3.2 GHz Intel Core i7 CPU personal computer with 8 GB RAM. In the following parts, the different results are validated and discussed.

a. Power generation and LMP

Fig. **2(a)** presents the dispatch plots of all generators at the day-ahead stage, and the right axis in this figure shows the day-ahead electricity price for the operating horizon. Note that load demand bid, WTs and PVs offer are 0.28($/kWh), 0.05($/kWh), and 0.045($/kWh), respectively and other µM participants data are available in Table IV. To simplify the analysis of the unit commitment and IMG's electricity price, the operational horizon is divided into four parts, including the pre-first peak period (PFPP), first peak period (FPP), second peak period (SPP) and post-second peak period (PSPP).

PFPP:

As it is clear, the G1 and G4 units with the lowest marginal costs are committed for the whole operating horizon. Regarding Fig. **2(a)**, in the PFPP, with the constant commitment of DGs, the price remained around 0.21 ($/kWh). In this period, as off-peak hours, the charging rate of the batteries is higher than their discharge, and the batteries are discharged only when approaching the peak hours. In addition, according to Fig. **2(b)**, the reactive power generation follows the load profile, and the DGs are dispatched to supply the demanded reactive load with the lowest reactive reserve provision cost.

FPP:

The 273% increase in load demand in this period leads to the commitment of G2 and G5 to meet the power balance constraint. By comparing the FPP in Fig. **2(a)** and Fig. **2(b)**, it can be understood that the LMP variations are matched with the load profile and the DGs' active power generation. Therefore, the LMP in peak hours (6-8) becomes close to the bid of the loads 0.28($/kWh). As can be seen in Fig. **2(b)** and Fig. **2(d)**, unlike the previous period with the higher charging rate, the batteries have only discharged power in this period. The reactive power generation follows the load profile, and all committed units are participated to supply reactive power.

SPP:

The electricity price comparison in FPP and SPP reveals that, unlike the FPP in which the LMP follows the load profile variations, the electricity price has been constant during SPP. The reason is that the total generated active power of RES has grown by 128% during SPP compared to the previous interval. This increase in the power generation of renewable resources reduces the participation of other units to supply active and reactive power and thus lowers the price. In other words, although the load demand grows during hours 10-12, the increasing available power of RES eliminates any need to change in DGs' commitment. In hours 13-15, the demanded load and RESs' output active power gradually decrease, so the electricity price and DGs' commitment remain constant throughout the SPP. Investigating the batteries' status shows that, like the previous on-peak period, the batteries have only discharged power in this interval.

PSPP:

Through the PSPP, the peak of the load has decreased by 30% compared to the previous period. So, it can be seen that G2 is committed at hours 16-20 with its minimum power. Therefore, the LMP during these hours remains constant. The output power unavailability of Wind turbines and PVs at t=21 leads to load supply by G1, G4, and ESS. Consequently, like the peak hours in FPP, the LMP gets close to the bid of the loads. After t=21, the load demand gradually decreases, and the LMP decreases accordingly. Since this period is considered off-peak, the charging rate of batteries is higher than their discharge, and the reactive power generation follows the load profile.

b. Reserve management & frequency

The scheduled active-reactive power reserves for different units are shown in Fig. **4(a)** and Fig. **4(b)**, respectively. Depending on the power balance constraint in the second stage, the upward and downward active-reactive reserves are provided. The active power reserves are not only responsible for meeting the power imbalances at the second stage, but also they are responsible for keeping the IMG's frequency within the predefined ranges at hierarchical control levels.

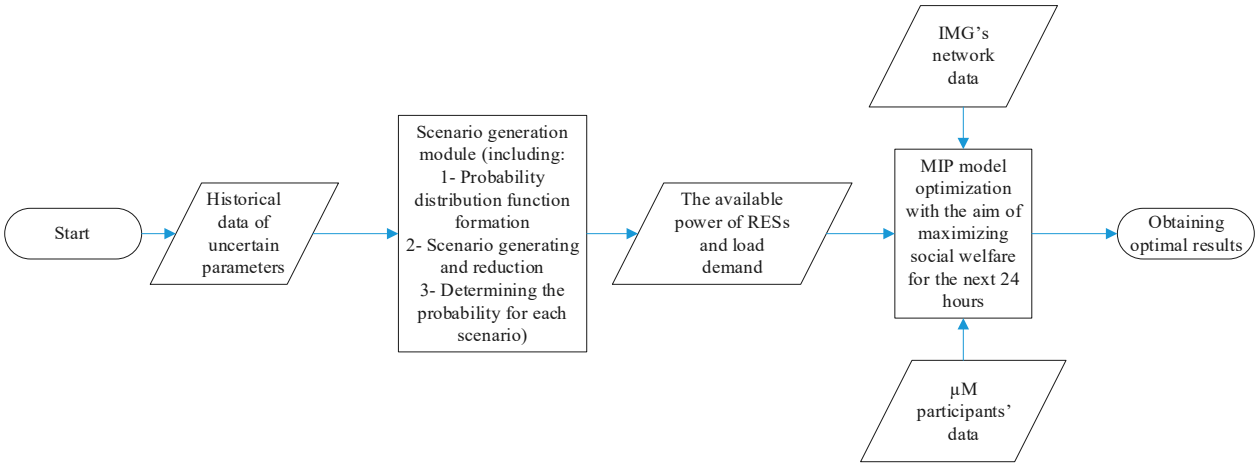

Fig. 1: Procedure of the proposed µM model

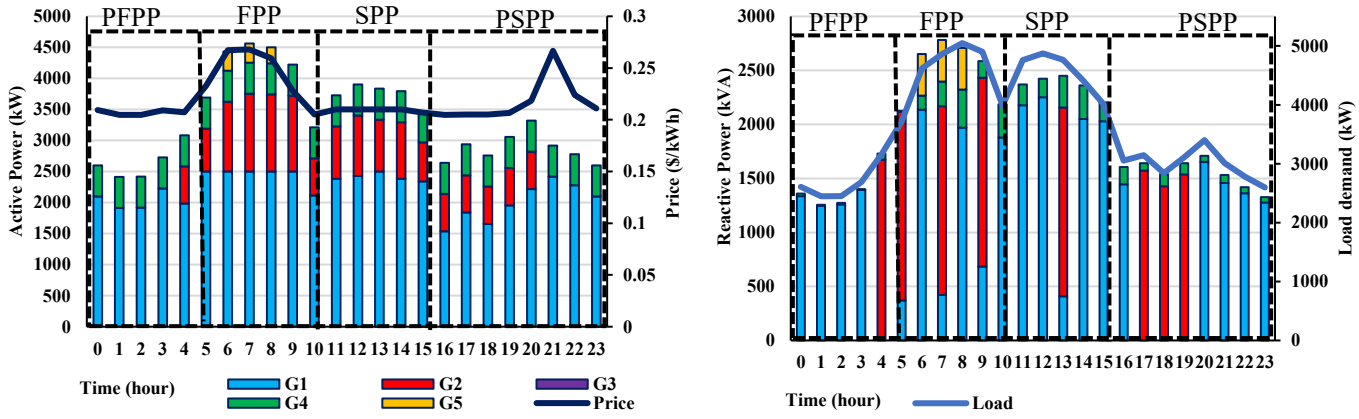

(a) (b)

Fig. 2: (a) Active power dispatch plot of all generators and electricty price. (b) Reactive power dispach plot and load profile.

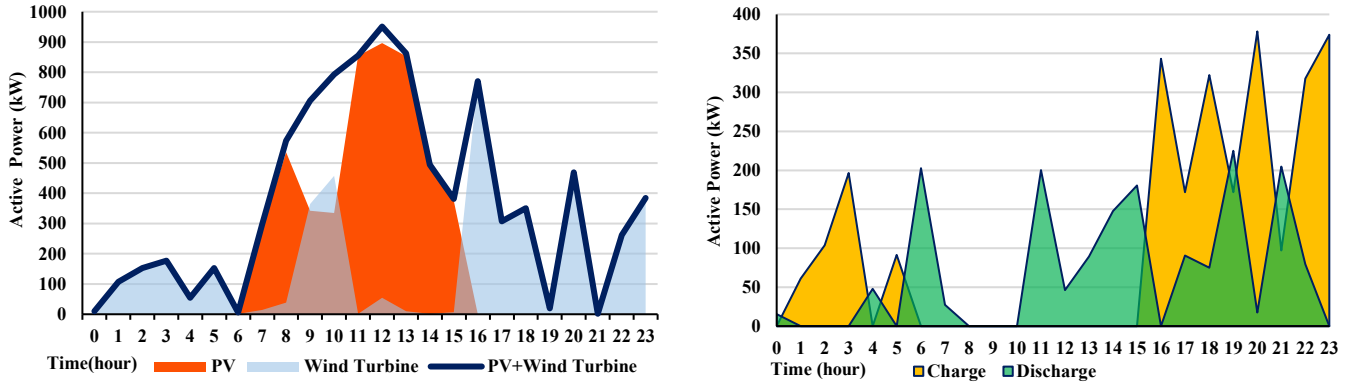

(a) (b)

Fig. 3: (a) Active power of RES. (b) Commulative charging and discharging status of all batteries.

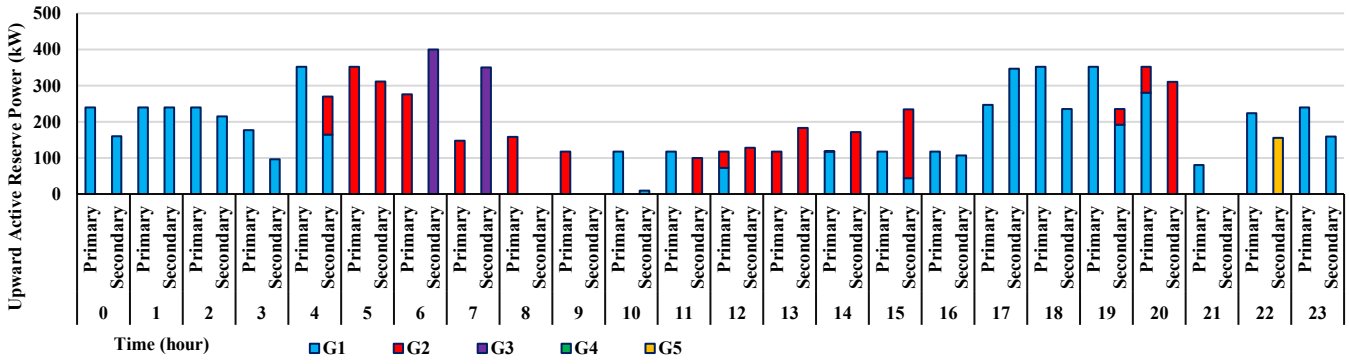

(a)

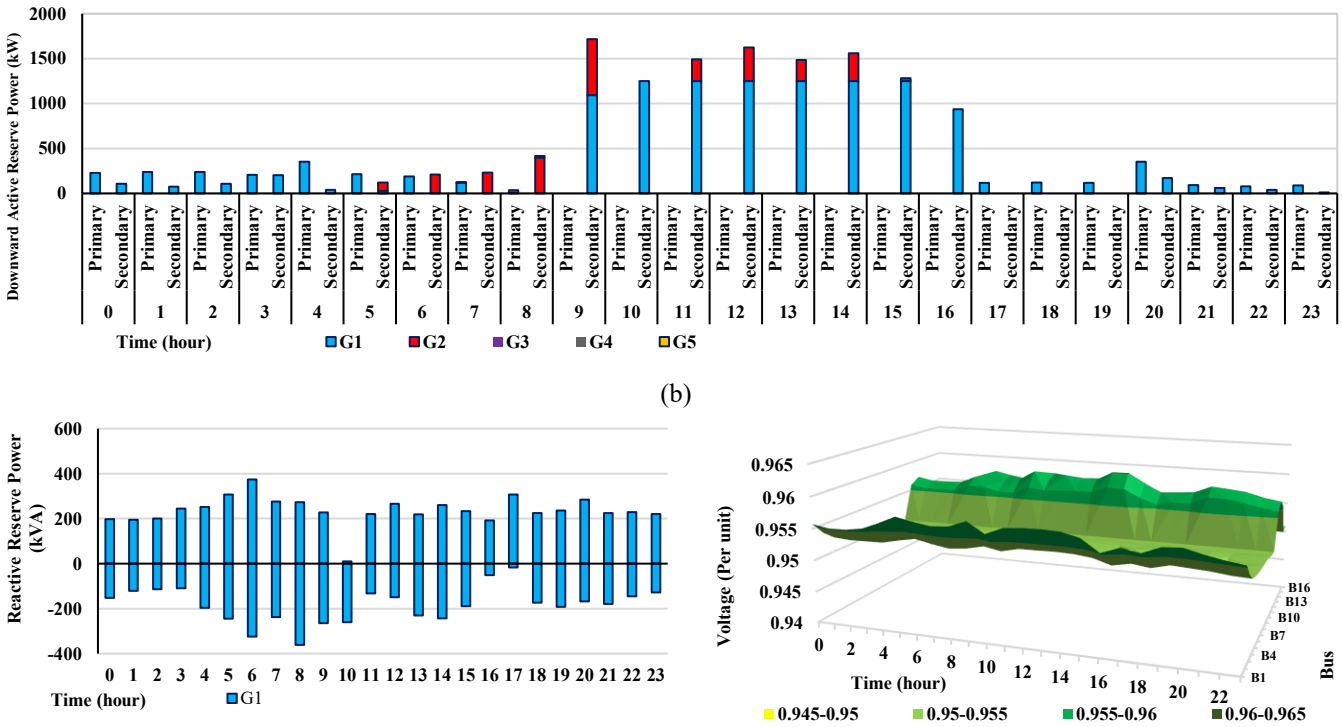

Fig. 4: (a) Scheduled upward active reserve power. (b) Scheduled downward active reserve power. (c) Scheduled up/downward reactive reserve power. (d) Voltage profile of IMG's network.

It should be noted that each unit's maximum reserve capacity is 50% of that unit's capacity, and the reserve powers are allocated to different generating units considering their reserve provision costs and available generation capacity. By comparing Fig. **2(a)** and Fig. **4(a)**, it could be understood that since the G4 has the lowest generation cost and highest reserve provision cost, it has been dispatched at the day ahead stage with its total capacity and no active reserve power is allocated to this unit. In addition, since the G1 has the second lowest generation cost and the lowest reserve provision cost, the active reserve power is allocated to this unit for most of the operating hours. In the rest of the operating hours, the active reserve power is allocated to the other units (including G2, G3, and G5) depending on the power imbalances and the IMG's frequency range.

As depicted in Fig. **3(a)** and Fig. **3(b)**, in hours 10-15, the second peak of load and maximum generation of RES pose more uncertainties to µM, and more power reserves are scheduled in SPP. Nevertheless, since it has been assumed that RESs work under a power factor of 0.95, these sources have a minor contribution to supplying reactive power. Therefore, it poses less uncertainty to µM than active power, so less reactive reserve power is needed. Fig. **4(c)** shows the scheduled upward reactive power reserves with positive sign while downward reactive power reserves are depicted with negative sign. As it is clear, since the DGs are scheduled to supply the reactive load demand with the lowest reactive reserve provision cost, reactive reserve powers are allocated to G1for the next 24 hours.

It can be seen in Fig. **4(a)** that, during the whole operating horizon, primary active reserves power are scheduled for different units. This point stems from the fact that a significant part of frequency fluctuations is compensated at the primary control level. However, more amount of downward secondary active reserve power is scheduled during the first and second peak hours. The reason is that most of the units with high generation capacity and cheaper costs are committed to supplying the day-ahead load demand during these hours. In addition, the reserve provision cost of the secondary reserve is lower than the primary reserve, and this amount of reservation should meet power balance constraint at the second stage for all the scenarios. For instance, in ω_1, with a 26% increase in the generation of RESs and 14% decrease of load demand compared to the day-ahead stage, the downward delivered active power deviation is $r^{Dn}_{g_1,t_{11},\omega_1,sec}$ =1.25 MW, which leads to 1.25 MW downward allocated active reserve power $RD_{g_1,t_{11},sec}$ =1.25 MW.

To verify the effect of fast start and frequency security constraints in hierarchical control level, the IMG's steady-state frequencies in primary and secondary control levels for ω_5 are presented in Fig. **5(a)**. Also, the IMG's frequency without considering frequency security constraint is shown in Fig. **5(b)**. Note that the allowable frequency excursions in primary and secondary control level are 100 mHz and 300 mHz, respectively.

Fig. **5(b)** perfectly depicts the role of frequency security constraints and scheduling sufficient amount of reserve to keep the IMG's frequency within the predefined ranges. In other words, when the IMG's frequency increases from the nominal value (i.e., 50 Hz), the scheduled downward reserves should compensate for the positive frequency fluctuations. In contrast, the scheduled upward reserves are used to mitigate the negative frequency fluctuations. For instance, as shown in Fig. **4(b)**, not considering the suitable amount of primary and secondary reserve at t=22 has led to excessive frequency deviation from its nominal value.

According to Fig. **4(a)** and Fig. **4(b)**, the frequency without security constraints is 49.60 Hz at t=22, while considering the suitable primary and secondary reserve ($RU_{g_1,t_{22},pri}$ =223 kW

and $RU_{g_3,t_{22},sec}$ =150 kW) will keep the primary and secondary frequency equal to 49.757 Hz and 49.933 Hz, respectively. By comparing Fig. **4(a)** and Fig. **2(a)**, it is evident that although units G3 and G5 are not committed at the day-ahead stage, the secondary active reserves are scheduled for these units at t=6,7 and 22. This point stems from the fact that the secondary control level, as formulated earlier, is able to use the fast start ability to add new units at the balancing stage. The fast start results in different scenarios are available in Table III. A comparison of Table IV, Fig. **4(a)** and Fig. **5(a)** shows that the use of fast start capability in ω_5 at t=7 and t=22 will mitigate negative frequency fluctuations and preserve frequency in the predefined range. Table I shows the summary of results for 3 cases.

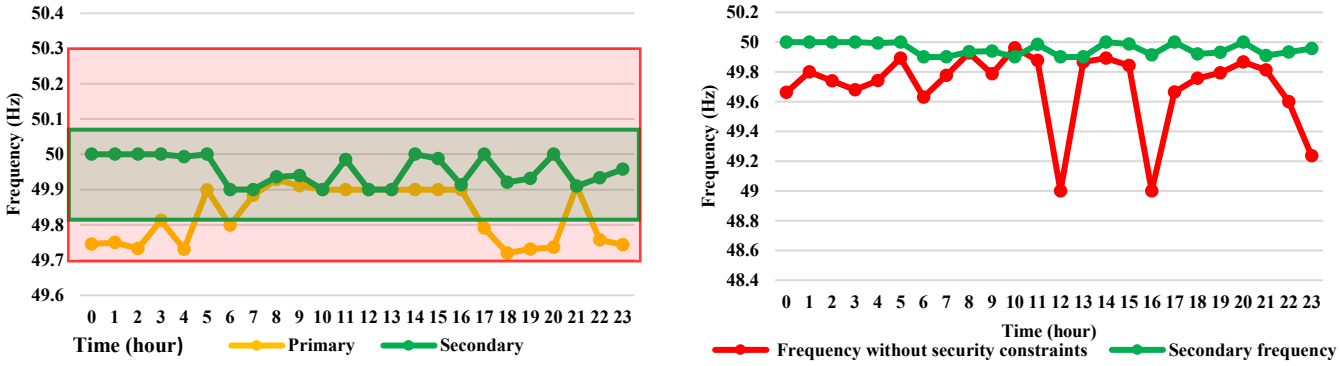

(a) (b)

Fig. 5: (a) IMG's frequency with frequency security constraints and fast start. (b) Comparison of IMG's frequency in secondary control level and without security constraints.

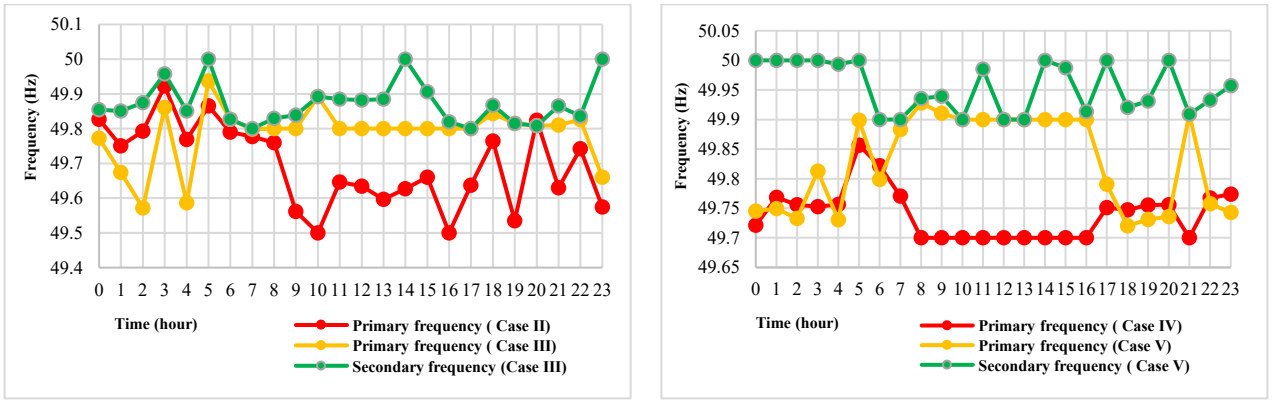

Fig.6: Comparison of the IMG's frequency in different operational cases for (a) 500 mHz primary and 200 mHz secondary frequency range. (b) 300 mHz primary and 100 mHz secondary frequency range.

TABLE I: SUMMARY OF RESULTS FOR CIGRE IMG

Case	Fast start	Frequency security constraints	Social welfare [$]	Reserve provision cost [$]	Day-ahead active power supply cost [$]	Computation time [s]
I	-	-	8632	173	15080	1267
II	-	✓	8545	397	15618	6417
III	✓	✓	8572	401	15570	10921

Table II: COMPARISON OF DIFFERENT OPERATIONAL CASES

Case	Frequency range	Hierarchical control levels		Social welfare [$]	Computation time [s]
		Primary	Secondary		
I	Primary=500 mHz Secondary=200 mHz	×	×	8632	1267
II		✓	×	8554	5417
III		✓	✓	8629	9832
IV	Primary=300 mHz Secondary=100 mHz	✓	×	8545	6417
V		✓	✓	8572	10921

TABLE III: GENERATORS' DATA

Unit	Bus	$C^{P}_{x,t}$ [$/kWh]	$C^{R,P}_{g,t,pri}$ [$/kWh]	$C^{R,P}_{g,t,sec}$ [$/kWh]	$C^{R,Q}_{g,t}$ [$/kVA.h]	r_g [mHz/kW]
G1	1	0.197	0.029	0.0097	0.0002	1.5
G2	1	0.226	0.034	0.011	0.0003	2.67
G3	1	0.253	0.038	0.012	0.0004	4.68
G4	13	0.15	0.075	0.025	0.0004	7.5
G5	9	0.253	0.068	0.023	0.0003	12

In the first case of Table I, neither fast start nor frequency constraints are not considered. Although the SW has a higher value, the secure operation is not ensured in this case. In the second case, the frequency security constraints which guarantee the secure operation are included, but it will lead to a 1.01% decrease in SW. Finally, both fast start and security constraints are considered in the third case. As evident in this case, the secure operation is guaranteed in addition to improvement in SW. Therefore, it can be seen that using the fast start capability is a cost-effective way to keep the frequency within the desired range without the need to involve expensive units at the day-ahead stage.

In order to evaluate the effects of hierarchical control structure on the IMG's frequency and SW, different operational cases are examined as depicted in Table II. In the first case, neither the primary control level nor the secondary control level is not considered. Case II-V provides the possibility to assess the effects of each control level on the IMG's frequency and SW. As Fig. **5(b)** represents, not considering the frequency security constraints and primary control level in case I leads to a lower frequency value than 49.7 Hz for eight hours, which is the maximum allowable primary frequency excursion. Although SW is higher in case I compared to case II, secure operation is not ensured. In case II, only the primary control level is considered with a 500 mHz frequency range. As shown in Fig. **6(a)**, in this case, the IMG's frequency is lower than 49.7 Hz for 12 hours, and the SW equals 8554$.

On the other hand, in case III, both hierarchical control levels are considered with 500 mHz and 200 mHz frequency ranges. The results in Fig. **6(a)** show that the primary frequency excursion in case III with both control levels, is less than primary frequency excursions in case II during the 78% of the operating horizon. In other words, the results demonstrate that considering both control levels leads to less frequency excursions from the nominal value (Secondary frequency in case III) and leads to less primary frequency excursions compared to case II, in which only the primary control level is considered. In addition, regarding Table II, considering the joint primary and secondary control levels leads to more SW value than case II.

In case IV and case V, the predefined frequency ranges are gotten tighter for both control levels. As depicted in Fig. **6(b)**, in case IV, the IMG's frequency is at its lowest allowable value for 10 hours, and the social welfare equals 8545$. In addition, the results show the primary frequency excursion in case V with both control levels is less than primary frequency excursions in case IV during 62.5% of the operating horizon and for the rest of the hours has a very close value to the primary frequency in case IV. Like case II and case III, in these cases, hierarchical control levels can lead to more values of SW compared to cases in which only the primary control level is considered. In addition, according to Table II, it could be seen that considering both hierarchical control levels may lead to higher social welfare compared to when only primary control is included, even with tighter frequency ranges (case II vs. case V).

TABLE IV: FAST START RESULTS

Unit	Time	Scenarios					
		ω_5	ω_{10}	ω_{11}	ω_{12}	ω_{13}	ω_{14}
G3	t=6	-	✓	✓	✓	✓	✓
G3	t=7	✓	-	-	-	-	-
G5	t=22	✓	✓	✓	✓	✓	✓

IV. CONCLUSIONS

This paper presented a novel Micro-Market model for isolated microgrids that aims to maximize social welfare during the next 24 hours. The hierarchical control structure of an isolated microgrid, including primary and secondary control levels, is accurately modeled in a two-stage stochastic framework. The results showed that implementing the proposed model can optimally schedule active-reactive power, and thanks to a bidirectional AC power flow, all market participants can exchange energy through an optimal strategy for the isolated microgrid. In addition, the simulation result demonstrated that the optimal scheduling of active-reactive reserve power not only copes with operational uncertainties but also preserves the primary and secondary frequency in the predefined ranges. Furthermore, the results indicated that considering the technical challenges and capabilities of isolated microgrids, such as the fast start capability or changing the set-points in the secondary control level, can provide secure operation and the possibility of local trade. Indeed, implementing the Micro-Market platform is not only compatible with the technical issues of isolated microgrids but also uses the potential of these networks to provide reliable energy and keep the profits in the microgrid community.

REFERENCES

[1] Y. Xia *et al.*, "A Safe Policy Learning-Based Method for Decentralized and Economic Frequency Control in Isolated Networked-Microgrid Systems," *IEEE Transactions on Sustainable Energy,* pp. 1-1, 2022, doi: 10.1109/TSTE.2022.3178415.

[2] W. Mendieta and C. A. Cañizares, "Primary Frequency Control in Isolated Microgrids Using Thermostatically Controllable Loads," *IEEE Transactions on Smart Grid,* vol. 12, no. 1, pp. 93-105, 2021, doi: 10.1109/TSG.2020.3012549.

[3] S. Córdova, C. A. Cañizares, L. Á, and D. E. Olivares, "Frequency-Constrained Energy Management System for Isolated Microgrids," *IEEE Transactions on Smart Grid,* pp. 1-1, 2022, doi: 10.1109/TSG.2022.3170871.

[4] B. V. Solanki, K. Bhattacharya, and C. A. Cañizares, "A Sustainable Energy Management System for Isolated Microgrids," *IEEE Transactions on Sustainable Energy,* vol. 8, no. 4, pp. 1507-1517, 2017, doi: 10.1109/TSTE.2017.2692754.

[5] " How to Make Modern Energy Access Universal?," *IEA (2010), Energy poverty, IEA, Paris https://www.iea.org/reports/energy-poverty-how-to-make-modern-energy-access-universal,* 2010.

[6] H. Mahmood and F. Blaabjerg, "Autonomous Power Management of Distributed Energy Storage Systems in Islanded Microgrids," *IEEE Transactions on Sustainable Energy,* pp. 1-1, 2022, doi: 10.1109/TSTE.2022.3156393.

[7] B. V. Solanki, C. A. Cañizares, and K. Bhattacharya, "Practical Energy Management Systems for Isolated Microgrids," *IEEE Transactions on Smart Grid,* vol. 10, no. 5, pp. 4762-4775, 2019, doi: 10.1109/TSG.2018.2868130.

[8] H. Moradi, M. Esfahanian, A. Abtahi, and A. Zilouchian, "Optimization and energy management of a standalone hybrid

microgrid in the presence of battery storage system," *Energy,* vol. 147, pp. 226-238, 2018.
[9] J. D. Lara, D. E. Olivares, and C. A. Cañizares, "Robust Energy Management of Isolated Microgrids," *IEEE Systems Journal,* vol. 13, no. 1, pp. 680-691, 2019, doi: 10.1109/JSYST.2018.2828838.
[10] D. E. Olivares, J. D. Lara, C. A. Cañizares, and M. Kazerani, "Stochastic-Predictive Energy Management System for Isolated Microgrids," *IEEE Transactions on Smart Grid,* vol. 6, no. 6, pp. 2681-2693, 2015, doi: 10.1109/TSG.2015.2469631.
[11] M. Nemati, M. Braun, and S. Tenbohlen, "Optimization of unit commitment and economic dispatch in microgrids based on genetic algorithm and mixed integer linear programming," *Applied Energy,* vol. 210, pp. 944-963, 2018/01/15/ 2018, doi: https://doi.org/10.1016/j.apenergy.2017.07.007.
[12] P. García, J. P. Torreglosa, L. M. Fernández, F. Jurado, R. Langella, and A. Testa, "Energy management system based on techno-economic optimization for microgrids," *Electric Power Systems Research,* vol. 131, pp. 49-59, 2016/02/01/ 2016, doi: https://doi.org/10.1016/j.epsr.2015.09.017.
[13] L. I. Minchala-Avila, L. Garza-Castañon, Y. Zhang, and H. J. A. Ferrer, "Optimal Energy Management for Stable Operation of an Islanded Microgrid," *IEEE Transactions on Industrial Informatics,* vol. 12, no. 4, pp. 1361-1370, 2016, doi: 10.1109/TII.2016.2569525.
[14] M. Javidsharifi, T. Niknam, J. Aghaei, M. Shafie-khah, and J. P. S. Catalão, "Probabilistic Model for Microgrids Optimal Energy Management Considering AC Network Constraints," *IEEE Systems Journal,* vol. 14, no. 2, pp. 2703-2712, 2020, doi: 10.1109/JSYST.2019.2927437.
[15] Z. Liu, S. Liu, Q. Li, Y. Zhang, W. Deng, and L. Zhou, "Optimal Day-ahead Scheduling of Islanded Microgrid Considering Risk-based Reserve Decision," *Journal of Modern Power Systems and Clean Energy,* vol. 9, no. 5, pp. 1149-1160, 2021, doi: 10.35833/MPCE.2020.000108.
[16] N. K. Paliwal, A. K. Singh, and N. K. Singh, "A day-ahead optimal energy scheduling in a remote microgrid alongwith battery storage system via global best guided ABC algorithm," *Journal of Energy Storage,* vol. 25, p. 100877, 2019/10/01/ 2019, doi: https://doi.org/10.1016/j.est.2019.100877.
[17] A. Hussain, S. Hasan, S. Patil, and W. Shireen, "Fast Frequency Regulation in Islanded Microgrid Using Model-Based Load Estimation," *IEEE Transactions on Energy Conversion,* vol. 36, no. 4, pp. 3188-3198, 2021, doi: 10.1109/TEC.2021.3076784.
[18] N. Rezaei, M. Mazidi, M. Gholami, and M. Mohiti, "A new stochastic gain adaptive energy management system for smart microgrids considering frequency responsive loads," *Energy Reports,* vol. 6, pp. 914-932, 2020/11/01/ 2020, doi: https://doi.org/10.1016/j.egyr.2020.04.021.
[19] Í. Munné-Collado, E. Bullich-Massagué, M. Aragüés-Peñalba, and P. Olivella-Rosell, "Local and micro power markets," *Micro and local power markets,* pp. 37-96, 2019.
[20] E. Mengelkamp, J. Gärttner, K. Rock, S. Kessler, L. Orsini, and C. Weinhardt, "Designing microgrid energy markets: A case study: The Brooklyn Microgrid," *Applied Energy,* vol. 210, pp. 870-880, 2018.
[21] S. Pullins, "Why microgrids are becoming an important part of the energy infrastructure," *The Electricity Journal,* vol. 32, no. 5, pp. 17-21, 2019/06/01/ 2019, doi: https://doi.org/10.1016/j.tej.2019.05.003.
[22] K. Antoniadou-Plytaria, D. Steen, L. A. Tuan, O. Carlson, and M. A. F. Ghazvini, "Market-Based Energy Management Model of a Building Microgrid Considering Battery Degradation," *IEEE Transactions on Smart Grid,* vol. 12, no. 2, pp. 1794-1804, 2021, doi: 10.1109/TSG.2020.3037120.
[23] C. Mu *et al.*, "A Decentralized Market Model for a Microgrid with Carbon Emission Rights," *IEEE Transactions on Smart Grid,* pp. 1-1, 2022, doi: 10.1109/TSG.2022.3173520.
[24] D. Prudhviraj, P. B. S. Kiran, and N. M. Pindoriya, "Stochastic Energy Management of Microgrid with Nodal Pricing," *Journal of Modern Power Systems and Clean Energy,* vol. 8, no. 1, pp. 102-110, 2020, doi: 10.35833/MPCE.2018.000519.
[25] M. H. K. Tushar and C. Assi, "Optimal Energy Management and Marginal-Cost Electricity Pricing in Microgrid Network," *IEEE Transactions on Industrial Informatics,* vol. 13, no. 6, pp. 3286-3298, 2017, doi: 10.1109/TII.2017.2712652.
[26] S. Bjarghov *et al.*, "Developments and challenges in local electricity markets: A comprehensive review," *IEEE Access,* vol. 9, pp. 58910-58943, 2021.
[27] S. C. Doumen, P. Nguyen, and K. Kok, "Challenges for large-scale Local Electricity Market implementation reviewed from the stakeholder perspective," *Renewable and Sustainable Energy Reviews,* vol. 165, p. 112569, 2022.
[28] S. Stoft, *Power system economics: designing markets for electricity*. IEEE press Piscataway, 2002.
[29] M. Shafie-Khah, P. Siano, D. Z. Fitiwi, N. Mahmoudi, and J. P. S. Catalão, "An Innovative Two-Level Model for Electric Vehicle Parking Lots in Distribution Systems With Renewable Energy," *IEEE Transactions on Smart Grid,* vol. 9, no. 2, pp. 1506-1520, 2018, doi: 10.1109/TSG.2017.2715259.
[30] C. Ruiz, A. J. Conejo, and S. A. Gabriel, "Pricing Non-Convexities in an Electricity Pool," *IEEE Transactions on Power Systems,* vol. 27, no. 3, pp. 1334-1342, 2012, doi: 10.1109/TPWRS.2012.2184562.
[31] J. M. Morales, A. J. Conejo, and J. Pérez-Ruiz, "Economic valuation of reserves in power systems with high penetration of wind power," *IEEE Transactions on Power Systems,* vol. 24, no. 2, pp. 900-910, 2009.
[32] U. Tamrakar, D. Shrestha, M. Maharjan, B. P. Bhattarai, T. M. Hansen, and R. Tonkoski, "Virtual inertia: Current trends and future directions," *Applied Sciences,* vol. 7, no. 7, p. 654, 2017.
[33] P. Rabbanifar and S. Jadid, "Stochastic multi-objective security-constrained market-clearing considering static frequency of power system," *International Journal of Electrical Power & Energy Systems,* vol. 54, pp. 465-480, 2014.
[34] R. Bahmani, H. Karimi, and S. Jadid, "Stochastic electricity market model in networked microgrids considering demand response programs and renewable energy sources," *International Journal of Electrical Power & Energy Systems,* vol. 117, p. 105606, 2020.

Tohid Abedi received his B.Sc. in electrical engineering as the top graduated student from Arak University, Arak, Iran, in 2017. He received his M.Sc. in power system engineering from the Isfahan University of Technology, Isfahan, Iran, in 2020. His research interests include energy management systems, microgrids, energy and reserve markets, power system optimization, frequency control and electric vehicles.

G. Reza Yousefi (M'03) received the B.Sc. degree in electrical engineering from the Isfahan University of Technology, Isfahan, Iran, in 1994 and the M.Sc. and Ph.D. degrees in electrical engineering from Tarbiat Modares University, Tehran, Iran, in 1997 and 2001, respectively. He has over 25 years of industry and academic experience in transmission system planning, power systems operations, reactive power planning, electricity markets and optimization. He was a senior electrical engineer at PG&E (California, USA). Also, he was a senior electrical engineer at Midwest Service Center (Indiana, USA) involved with design, uprate and performance improvement of large industrial motors and generators. His research interests are power systems operation and planning as well as restructuring and smart grids.

Miadreza Shafie-khah (SM'17) received his first PhD in electrical engineering from Tarbiat Modares University, Tehran, Iran. He received his second PhD in electromechanical engineering and first postdoc from the University of Beira Interior, Covilha, Portugal. He received his second postdoc from the University of Salerno, Salerno, Italy. Currently, he is a Professor (tenure-track) at the University of Vaasa, Vaasa, Finland. He is an Editor of the Ieee Transactions on Sustainable Energy, IEEE Systems Journal, IEEE Access, IEEE Open Access Journal of Power and Energy (OAJPE), Transactions on Intelligent Transportation Systems, and the guest Editor-in-Chief of the IEEE OAJPE. His research interests include electricity markets, power system optimization, demand response, electric vehicles, price and renewable forecasting.